APPLIED PHYSICS LETTERS 112, 051104 (2018)

A dissipative self-sustained optomechanical resonator on a silicon chip

J. G. Huang,[1,2,3,a)] Y. Li,[4,a)] L. K. Chin,[2] H. Cai,[3] Y. D. Gu,[3] M. F. Karim,[2] J. H. Wu,[1] T. N. Chen,[1] Z. C. Yang,[5] Y. L. Hao,[5] C. W. Qiu,[4] and A. Q. Liu[2,5,b)]
[1]*School of Mechanical Engineering, Xi'an Jiaotong University, Xi'an 710049, China and State Key Laboratory for Strength and Vibration of Mechanical Structures, Xi'an 710049, China*
[2]*School of Electrical & Electronic Engineering, Nanyang Technological University, Nanyang Avenue 50, Singapore 639798*
[3]*Institute of Microelectronics, A*STAR (Agency for Science, Technology and Research), 2 Fusionopolis Way, #08-02 Innovis Tower, Singapore 138634*
[4]*Department of Electrical and Computer Engineering, National University of Singapore, 4 Engineering Drive 3, 117583 Singapore*
[5]*School of Electronics Engineering & Computer Science, Peking University, Beijing 100871, China*

(Received 16 October 2017; accepted 19 January 2018; published online 30 January 2018)

In this letter, we report the experimental demonstration of a dissipative self-sustained optomechanical resonator on a silicon chip by introducing dissipative optomechanical coupling between a vertically offset bus waveguide and a racetrack optical cavity. Different from conventional blue-detuning limited self-oscillation, the dissipative optomechanical resonator exhibits self-oscillation in the resonance and red detuning regime. The anti-damping effects of dissipative optomechanical coupling are validated by both numerical simulation and experimental results. The demonstration of the dissipative self-sustained optomechanical resonator with an extended working range has potential applications in optomechanical oscillation for on-chip signal modulation and processing. *Published by AIP Publishing.* https://doi.org/10.1063/1.5009402

Optomechanical devices, which use light-matter interactions in nano-scale photonic structures, have been explored extensively in applications such as torque sensors,[1] non-volatile mechanical memory,[2] wavelength converters,[3] and high resolution accelerometers.[4] In particular, self-sustained optomechanical resonators,[5] which can be directly used for on-chip photonic clocks,[6] homodyne RF receivers,[7] and sub-carrier optical links,[8] are attracting more and more attention. Typically, there are two mechanisms being adopted in optomechanical resonators, i.e., dispersive[9] and dissipative[10] optomechanical couplings, which arise from optical cavity resonance frequency and cavity photon lifetime, respectively, depending on the displacement of mechanical resonators.

Previous investigations of self-sustained optomechanical resonators are based on dispersive optomechanical coupling[11] whereby self-oscillation in the linear regime requires a blue-detuned drive light relative to the optical resonance.[8] This limitation is overcome in highly nonlinear optomechanical resonators by introducing a modulated optical pump.[12] However, for practical applications, it is desirable to achieve self-oscillation in the linear regime without being limited by the blue-detuned light. In fact, the unique characteristics of dissipative optomechanical coupling can be used to overcome this limitation. For example, Wu *et al.* used a splitting optical cavity to generate a large dissipative coupling in torque and paddle beams,[1] Tsvirkun *et al.* demonstrated dissipative coupling in a vertically separated photonic crystal,[13] and Li *et al.* investigated dissipative coupling in a microdisk-waveguide design, in which a feeding waveguide is movable in-plane to generate dissipative coupling into the disk.[14] However, up to now, dissipative self-sustained optomechanical resonators are yet to be demonstrated.[15]

Here, we design, fabricate, and experimentally investigate a self-sustained optomechanical resonator on a silicon chip by introducing dissipative optomechanical coupling between a vertically offset bus waveguide and a racetrack optical cavity. Compared with conventional dispersive optomechanical systems, the self-oscillations induced by the dissipative mechanism can achieve a large working range (from the blue to red detuning regime) and a relatively low threshold power (70 μW). The self-sustained optomechanical resonator based on dissipative coupling can be used as an on-chip phonon source that consumes low power, which has high potential in compact signal processing or modulation applications.

Our dissipative optomechanical resonator consists of a racetrack optical cavity, a mechanical resonator, and a curved bus waveguide as shown in Fig. 1(a). The mechanical resonator is a double-clamped beam located at one arm of the optical racetrack cavity with a cross-section of $450 \times 220\,\mathrm{nm}^2$ and a length of $L = 20\,\mu$m. The mechanical resonator vibrates in the out-of-plane direction, which corresponds to fundamental mechanical modes. Other mechanical modes, which are either too small or in the much higher frequency range, are not discussed in the paper. The curved bus waveguide is coupled to the racetrack optical cavity with a gap of 200 nm. The device is fabricated in an SOI wafer by silicon nanophotonic technology with a 220-nm silicon structure layer.[16] The cross-section of the released region and the schematic of optomechanical coupling of the mechanical resonator are shown in Fig. 1(b). Although the mechanical resonator and the bus waveguide are both released from the substrate with a gap of 300 nm, the suspended double-clamped beam mechanical resonator in the

[a)]J. G. Huang and Y. Li contributed equally to this work.
[b)]Author to whom correspondence should be addressed: eaqliu@ntu.edu.sg

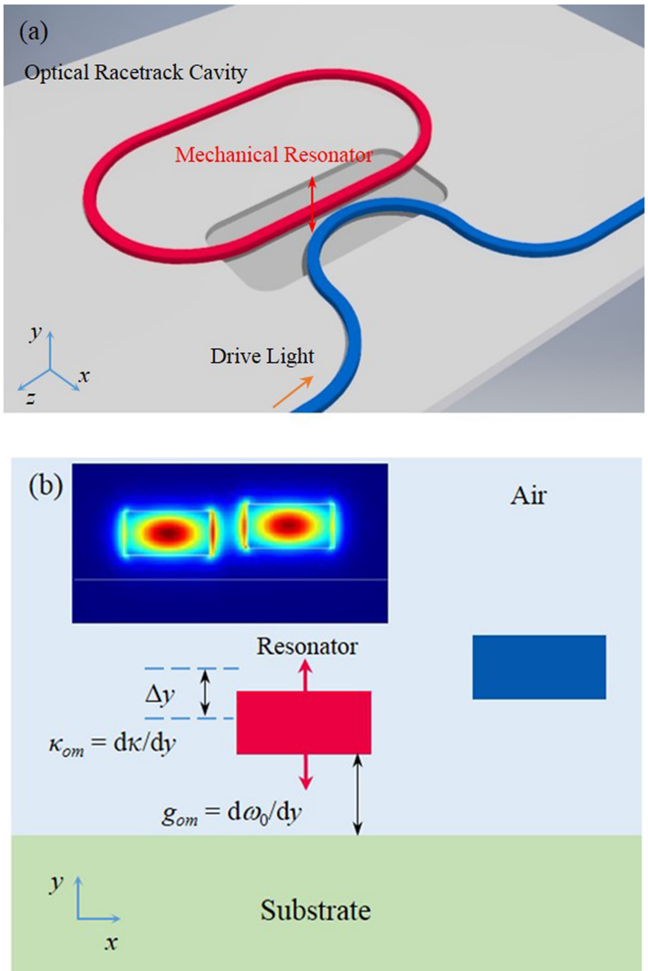

FIG. 1. (a) Schematic of optomechanical coupling between the curved input waveguide and the optical racetrack cavity. (b) Schematic of the cross-section of the released region. The inset is the finite element simulation result showing the E_x component of the optical fields in the waveguide being evanescently coupled to the optical racetrack cavity.

racetrack optical cavity is slightly lower than the bus waveguide with a vertical offset of Δy.

The dissipative and dispersive couplings in this optomechanical resonator arise from the out-of-plane vibrations of the mechanical resonator, altering the offset Δy between the mechanical resonator and the bus waveguide. When the mechanical resonator vibrates and move towards the substrate, the effective index of waveguides in the racetrack optical cavity increases, causing the decrease in optical resonance frequency ω_0. The dispersive coupling factor is defined as $g_{om} = d\omega_0/dy$. When the mechanical resonator vibrates and approaches the substrate, transmission from the bus waveguide to the optical cavity is reduced due to evanescent wave mismatch, which corresponds to the reduced external coupling rate κ_e. The dissipative coupling factor is defined as $\kappa_{om} = d\kappa_e/dy$. Thus, both the resonance frequency and external coupling rate of the optical cavity can be modulated by the mechanical resonator in this vertically offset design, resulting in the dispersive and dissipative couplings. It should be noted that the intrinsic dissipative coupling can be neglected because the mechanical vibration does not change the intrinsic coupling rate.

In the experiment, a broadband amplified spontaneous emission (ASE) light (ALS-CL-13) is first coupled into the bus waveguide through a grating coupler to characterize the transmission spectrum of the optical cavity, which is analysed using an optical spectrum analyser (AQ6370D).[17] The grating coupler is designed for TE mode transmission in the optical waveguide with a grating period of 630 nm and an etching depth of 130 nm.[18] The mechanical thermal noise (under a high vacuum environment, 2×10^{-6} Pa) is measured using a tunable laser (TSL 510) with polarization and power being controlled. The output signal is received by a photon detector and analysed using an oscilloscope (MDO4104B-3). The detailed experimental set-up is shown in Fig. 2(a). Based on the measured optical transmission spectrum as shown in Fig. 2(b), the optical racetrack cavity exhibits a high-quality factor of $Q_o = 7.96 \times 10^4$ at the resonance wavelength of $\lambda_o = 1591.33$ nm with a linewidth of $\delta\lambda = 20$ pm. The thermal mechanical noise is shown in Fig. 2(c), which exhibits two resonance peaks at $f_1 = 2.03$ MHz and $f_2 = 6.50$ MHz. The inset shows the finite element simulation of two fundamental mechanical modes of the mechanical resonator and suspended bus waveguide. The mechanical quality factor of the mechanical resonator and suspended bus waveguide is $Q_{m1} = 676$ and $Q_{m2} = 2096$ with mechanical linewidths of 3 kHz and 3.1 kHz, respectively.

We first give a theoretical derivation of the transduction mechanism. In the presence of dispersive and dissipative couplings, the intra-cavity mode amplitude a is described as[15]

$$\dot{a}(t) = (i(\Delta - g_{om}y) - (\kappa - \kappa_{om}y)/2)a(t) + (\kappa - \kappa_{om}y)\sqrt{n_{\max}}/2, \tag{1}$$

$$m_{eff}\ddot{y} + m_{eff}\gamma_m\dot{y} + m_{eff}\omega_m^2 y = \hbar g_{om}a^* a, \tag{2}$$

where $\Delta = \omega_0 - \omega$ is the frequency detuning, ω is the driving laser frequency, ω_0 is the optical cavity resonance frequency, g_{om} is the dispersive coupling, κ_{om} is the dissipative coupling, y is the displacement of the mechanical resonator, κ is the cavity linewidth, $n_{\max}$ is the maximum cavity photon number when the detuning is zero $n_{\max} = 4P_{in}\kappa_e/\kappa^2\hbar\omega$, κ_e is the external cavity linewidth, and P_{in} is the incident power. The total transmission is expressed as $T = (4(\Delta - g_{om}y)^2 + 4(\kappa/2 - \kappa_e)^2)/4(\Delta - g_{om}y)^2 + (\kappa - \kappa_{om}y)^2$. κ_e is estimated to be 0.47κ in our device by fitting the transmission spectrum. A shift in the y-direction dy will change the optical resonance frequency and coupling rate, resulting in a variation dT in the transmission spectrum, i.e., $dT = (g_{om}\partial T/\partial\Delta + \kappa_{om}\partial T/\partial\kappa_e)dy$, where $\partial T/\partial\Delta$ and $\partial T/\partial\kappa_e$ are the dispersive and dissipative transduction factors.[16] The measured power spectral density at mechanical frequency due to transmission fluctuations is expressed as[1]

$$S_p = \frac{(\eta P_{in}G)^2}{R}\frac{4k_bTQ_m}{m_{eff}(2\pi f_1)^3}\left(\frac{dT}{dy}\right)^2, \tag{3}$$

where $\eta \sim 0.3$ is the coupling efficiency of the grating coupler, $P_{in} \sim 10\,\mu$W is the estimated power in the bus waveguide, $G \sim 1 \times 10^4$ V/W is the detector gain factor, $k_b = 1.38 \times 10^{-23}$J K^{-1} is the Boltzmann constant,

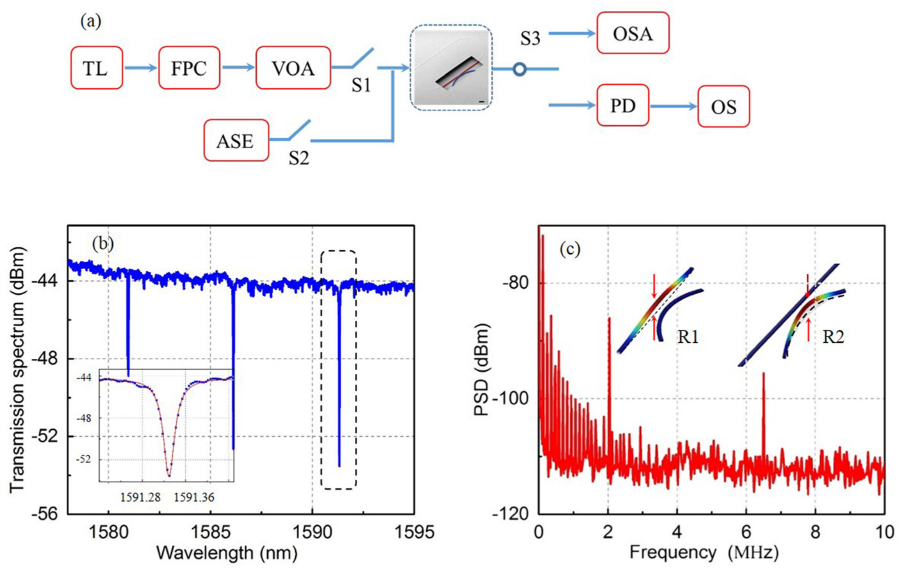

FIG. 2. (a) Schematic of the measurement set-up. TL, tunable laser; FPC, fiber polarization controller; VOA, variable optical attenuator; ASE, amplified spontaneous emission light; OSA, optical spectrum analyzer; PD, photon detector; OS, oscilloscope; and S1-S3, switch. (b) Transmission spectrum of the optical racetrack cavity. The inset is the fitting of optical resonance at 1591.33 nm. (c) Power spectrum density of the mechanical resonator. The inset is the finite element simulation of two fundamental mechanical modes.

$T = 293\,\mathrm{K}$ is the room temperature, Q_m is the mechanical quality factor, $R = 50\Omega$ is the load resistance, m_{eff} is the effective mechanical mass ($m_{eff} = 0.64\mathrm{pg}$), and f_1 is the mechanical frequency.

In the experiment, a low power light of $10\,\mu\mathrm{W}$ at wavelength λ_d is coupled into the devices. The transduction amplitude of measured power spectral density at the mechanical resonator as a function of wavelength detuning ($\Delta\lambda/\delta\lambda = (\lambda_d - \lambda_o)/\delta\lambda$)[19] is shown in Fig. 3(a). By fitting the measured experimental results using Eq. (3), the dispersive and dissipative coupling factors with $g_{om}/2\pi = 560\,\mathrm{MHz/nm}$ and $\kappa_{om}/2\pi = 109\,\mathrm{MHz/nm}$ are obtained, which are plotted as the blue and red dotted lines for clear illustration. In particular, the interference between the dispersive and dissipative couplings is also observed in the experiments. When the wavelength detuning ($\Delta\lambda/\delta\lambda$) is tuned from -2.8 to 2.8, the power spectrum density shows two peaks and the peak at detuning -0.5 is larger than that at detuning 0.5. The reason is that the dispersive and dissipative couplings have constructive interference $|g_{om}\partial T/\partial\Delta| + |\kappa_{om}\partial T/\partial\kappa_e|$ at blue detuning ($\Delta\lambda/\delta\lambda \le 0$) and destructive interference $|g_{om}\partial T/\partial\Delta| - |\kappa_{om}\partial T/\partial\kappa_e|$ at red detuning ($\Delta\lambda/\delta\lambda \ge 0$). To validate the vertical offset, the simulated transmission and dissipative optomechanical coupling as a function of the vertical offset are shown in Fig. 3(b). Since we have determined the dissipative optomechanical coupling as $\kappa_{om}/2\pi = 109\,\mathrm{MHz/nm}$, the vertical offset is estimated to be 36 nm. The vertical offset can be controlled in the fabrication process by introducing a residual stress in the silicon layer through silicon dioxide deposition on the backside of the wafer.

After characterizing the dissipative coupling factor, the optical power is increased to excite the mechanical resonator into self-oscillation. A numerical simulation is performed to gain an insight into the mechanism of self-oscillation induced by dissipative coupling. By combining the equations of optical cavity and mechanical resonator, the coupled equation is expressed as[20]

$$\dot{\tilde{a}}(\tilde{t}) = \Big(i(\tilde{\Delta} - \tilde{g}_{om}\tilde{y}) - (\tilde{\kappa} - \tilde{\kappa}_{om}\tilde{y})/2\Big)\tilde{a}(\tilde{t}) + (\tilde{\kappa} - \tilde{\kappa}_{om}\tilde{y})/2, \tag{4}$$

$$\ddot{\tilde{y}} + \tilde{\gamma}_m\dot{\tilde{y}} + \tilde{y} = J\tilde{a}\tilde{a}^*, \tag{5}$$

whereby the frequencies are normalized by ω_1, $\tilde{t} = \omega_1 t$, $\tilde{y} = g_{om}y/\omega_1$, $\tilde{a} = a/\sqrt{n_{\max}}$, $\tilde{\Delta} = \Delta/\omega_1$, $\tilde{g}_{om} = 1$, $\tilde{\kappa} = \kappa/\omega_1$,

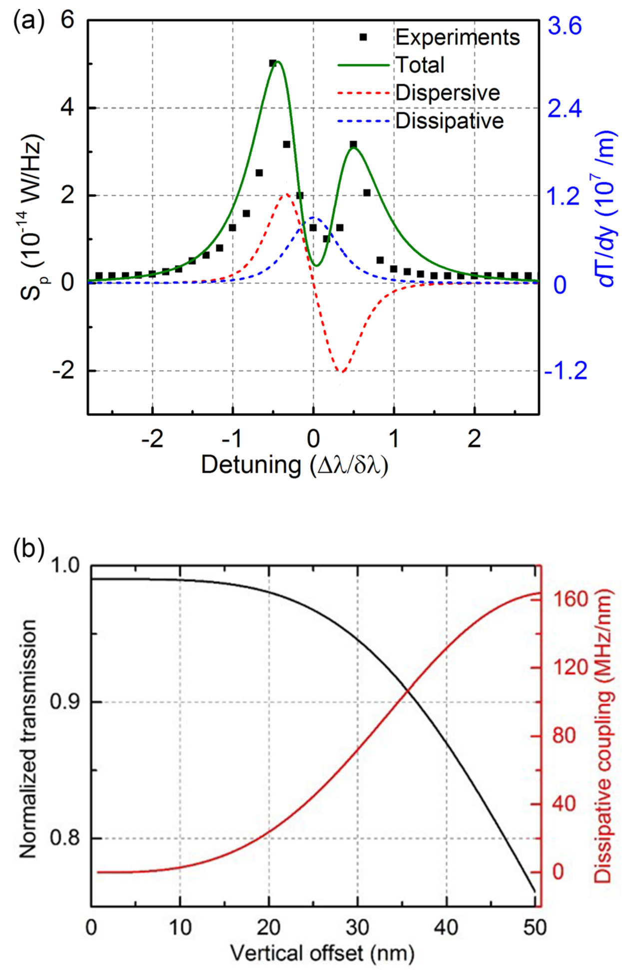

FIG. 3. (a) Measured power spectrum density at mechanical resonance as a function of wavelength detuning. The red (blue) dotted lines are simulated dispersive (dissipative) optomechanical coupling. The value of *y*-axes is calculated based on Eq. (3). (b) Simulated normalized transmission and dissipative coupling as a function of the vertical offset. The vertical offset of the mechanical resonator changes the transmission of the cavity due to evanescent wave mismatch.

$\tilde{\kappa}_{om} = \kappa_{om}/g_{om}$, $\tilde{\gamma} = \gamma_m/\omega_1$, $\omega_1 = 2\pi f_m$, and $J = 4\hbar n_{\max} {g_{om}}^2/m_{eff}{\omega_1}^3$ is the coupling strength. By setting $\tilde{\kappa}_{om} = 0$, the coupled equations are reduced to those that describe conventional dispersive optomechanical resonators. The simulated response of the mechanical resonator in the time domain at zero-detuning with $\tilde{\Delta} = 0$, $\tilde{g}_{om} = 1$, $\tilde{\kappa} = 100$, $J = 6$, and $\tilde{\gamma} = 1.5 \times 10^{-3}$ is shown in Fig. 4(a). Based on previous theoretical derivation[21] and experimental results,[22] the mechanical resonator will not be excited into self-oscillation when the detuning is on resonance, i.e., $\tilde{\Delta} = 0$, which agrees well with our simulated results. However, by setting $\tilde{\kappa}_{om} = 0.2$ with the other same parameters, the mechanical resonator steps into self-oscillation as shown in Fig. 4(b). By setting the detuning in the red-detuning regime, the self-oscillation still holds. The simulated results confirm that the dissipative coupling can effectively excite the mechanical resonator into self-oscillation from the blue to red-detuning regime, breaking the conventional limitation. We conclude that the total optical anti-damping factor can be expressed as $\gamma_{\text{total}} = \gamma_{\text{o}} + \gamma_{\text{e}}$, where γ_{o} and γ_{e} are the anti-damping factors provided by dispersive and dissipative couplings,[13,14] respectively. In the blue-detuning regime, both γ_{o} and γ_{e} compensate the intrinsic mechanical damping and contribute to self-oscillation. On the other hand, while in on-resonance or red-detuning, γ_{o} increases the mechanical damping and γ_{e} must be larger than γ_{o} and the intrinsic mechanical damping to excite the mechanical resonator into self-oscillation. As a result, the optomechanical resonator can operate from the blue to red detuning regime with the presence of dissipative coupling.

Finally, self-oscillation from the blue to red detuning regime is experimentally demonstrated. A blue detuned drive light at power $P_{\text{in}} = 100\,\mu$W is coupled into the optical racetrack cavity to introduce the optical anti-damping effects on the mechanical resonator. The measured power spectral density in the time and frequency domain as a function of wavelength detuning $\Delta\lambda/\delta\lambda$ from -3 to 1 is shown in Fig. 5(a). The time domain traces clearly show that the mechanical resonator steps into self-oscillation from $\Delta\lambda/\delta\lambda = -2.5$ and ends at $\Delta\lambda/\delta\lambda = 1$. To visualize the detuning process, the mechanical linewidth and frequency shift as a function of wavelength detuning are shown in Fig. 5(b). In the presence

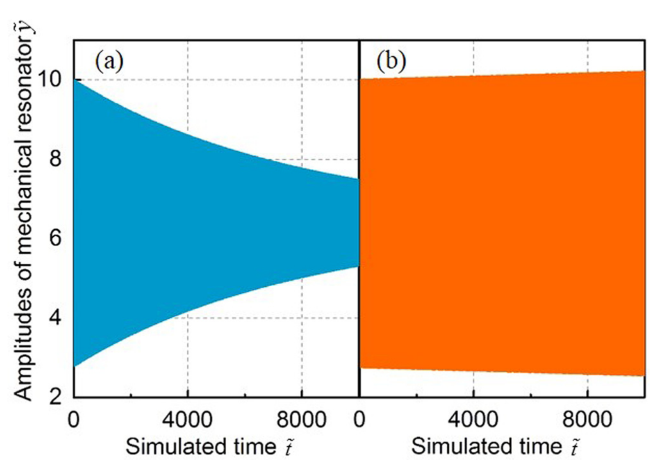

FIG. 4. Simulated response of the mechanical resonator at zero-detuning when dissipative coupling is set as (a) $\tilde{\kappa}_{om} = 0$ and (b) $\tilde{\kappa}_{om} = 0.2$ based on Eqs. (4) and (5).

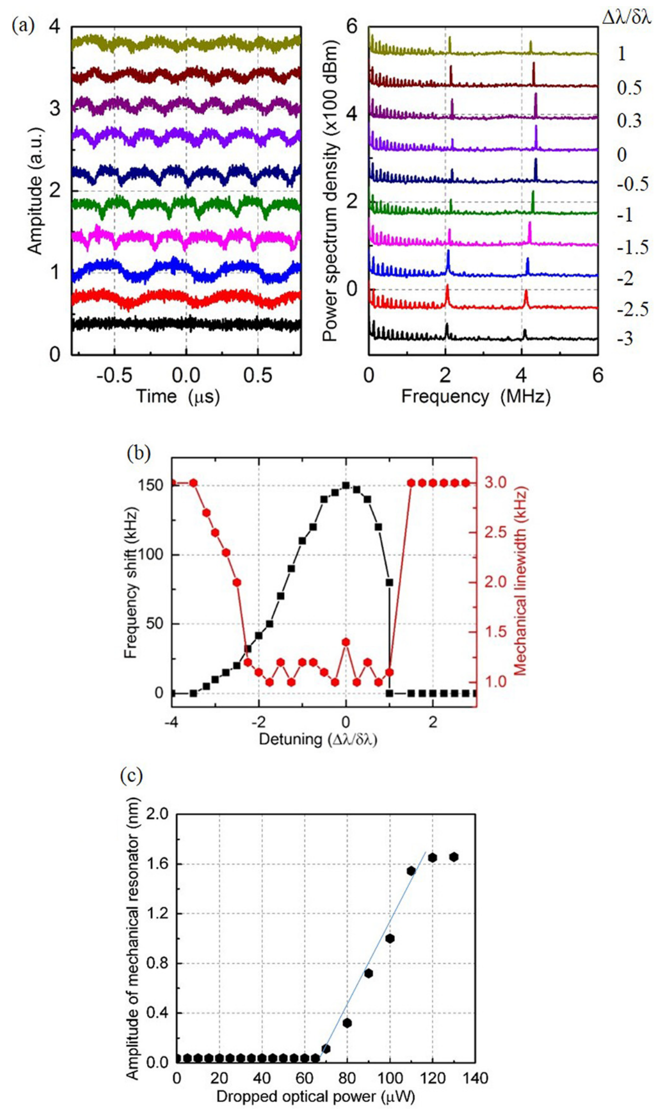

FIG. 5. (a) Signals in the time and frequency domain obtained from the photon detector when the wavelength detuning is controlled from -3 to 1. The curves are vertically offset for clear illustration. (b) Measured mechanical frequency shift and mechanical linewidth as a function of wavelength detuning. (c) Amplitude of the mechanical resonator as a function of dropped optical power at detuning -2. The threshold power is $70\,\mu$W.

of dissipative coupling, the mechanical resonator starts to self-oscillate from $\Delta\lambda/\delta\lambda = -2.5$ to 1 (mechanical linewidth decreased below 1.5 kHz)[23] and the frequency of the mechanical resonator is increased with the wavelength detuning, showing a maximum shift of 150 kHz at on-resonance detuning. It is noted that the mechanical nonlinearity and optomechanically induced Duffing nonlinearity start to play a role in the self-oscillation regime. We attribute this maximum on-resonance frequency shift to these nonlinear effects. The observed self-oscillations in detuning $\Delta\lambda/\delta\lambda$ from -2.5 to 1 confirm that the mechanical resonator can operate from the blue to red detuning regime with the presence of dissipative coupling. In particular, in the on-resonance and red-detuning regime, the self-oscillation totally depends on the dissipative coupling. The amplitudes of the mechanical resonator as a function of dropped optical power are shown in Fig. 5(c) with a maximum amplitude of 1650 pm. The threshold power $70\,\mu$W demonstrated in this design is modest in comparison with other state-of-the-art dispersive optomechanical oscillators [3.56 (Ref. 24)–127 μW].[24,25] In particular, we estimated that the optomechanical resonator can achieve a 10% reduction in the threshold power as compared with pure dispersive optomechanical coupling in the blue detuning regime by simulating Eqs. (4) and (5).

In conclusion, a dissipative self-sustained optomechanical resonator on a silicon chip is designed, fabricated, and experimentally demonstrated. By introducing dissipative optomechanical coupling between a vertically offset bus waveguide and a racetrack optical cavity, the self-oscillation is observed from blue detuning $\Delta\lambda/\delta\lambda = -2.5$ to red detuning $\Delta\lambda/\delta\lambda = 1$. The anti-damping effects of dissipative coupling are also investigated in both numerical simulation and experimental results. The demonstration of optomechanical oscillation with the extended working range provides a different way to investigate dissipative optomechanical coupling and will benefit potential applications of optomechanical oscillation in on-chip signal modulation and processing.[18]

This work was supported by Singapore National Research Foundation under the Incentive for Research & Innovation Scheme (1102-IRIS-05-01) and under the Competitive Research Program (NRF-CRP13-2014-01).

[1]M. Wu, A. C. Hryciw, C. Healey, D. P. Lake, H. Jayakumar, M. R. Freeman, J. P. Davis, and P. E. Barclay, Phys. Rev. X **4**, 021052 (2014).
[2]M. Bagheri, M. Poot, M. Li, W. P. Pernice, and H. X. Tang, Nat. Nanotechnol. **6**, 726 (2011).
[3]L. Tian and H. Wang, Phys. Rev. A **82**, 053806 (2010).
[4]A. G. Krause, M. Winger, T. D. Blasius, Q. Lin, and O. Painter, Nat. Photonics **6**, 768 (2012).
[5]F. Marquardt and S. M. Girvin, Physics **2**, 40 (2009).
[6]G. Anetsberger, R. Rivière, A. Schliesser, O. Arcizet, and T. J. Kippenberg, Nat. Photonics **2**, 627 (2008).
[7]M. Hossein-Zadeh and K. J. Vahala, IEEE Photonics Technol. Lett. **20**, 234 (2008).
[8]M. Hossein-Zadeh and K. J. Vahala, IEEE J. Sel. Top. Quantum Electron. **16**, 276 (2010).
[9]A. Jayich, J. Sankey, B. Zwickl, C. Yang, J. Thompson, S. Girvin, A. Clerk, F. Marquardt, and J. Harris, New J. Phys. **10**, 095008 (2008).
[10]A. Xuereb, R. Schnabel, and K. Hammerer, Phys. Rev. Lett. **107**, 213604 (2011).
[11]J. Roels, I. De Vlaminck, L. Lagae, B. Maes, D. Van Thourhout, and R. Baets, Nat. Nanotechnol. **4**, 510 (2009).
[12]A. G. Krause, J. T. Hill, M. Ludwig, A. H. Safavi-Naeini, J. Chan, F. Marquardt, and O. Painter, Phys. Rev. Lett. **115**, 233601 (2015).
[13]V. Tsvirkun, A. Surrente, F. Raineri, G. Beaudoin, R. Raj, I. Sagnes, I. Robert-Philip, and R. Braive, Sci. Rep. **5**, 16526 (2015).
[14]M. Li, W. H. Pernice, and H. X. Tang, Phys. Rev. Lett. **103**, 223901 (2009).
[15]A. Schliesser and T. J. Kippenberg, Adv. At., Mol., Opt. Phys. **58**, 207 (2010).
[16]J. Huang, H. Cai, Y. Gu, L. Chin, J. Wu, T. Chen, Z. Yang, Y. Hao, and A. Liu, Appl. Phys. Lett. **111**, 111102 (2017).
[17]M. Ren, J. Huang, H. Cai, J. M. Tsai, J. Zhou, Z. Liu, Z. Suo, and A.-Q. Liu, ACS Nano **7**, 1676 (2013).
[18]D. Van Thourhout and J. Roels, Nat. Photonics **4**, 211 (2010).
[19]G. S. Wiederhecker, L. Chen, A. Gondarenko, and M. Lipson, Nature **462**, 633 (2009).
[20]M. Poot, K. Fong, M. Bagheri, W. Pernice, and H. Tang, Phys. Rev. A **86**, 053826 (2012).
[21]K. Y. Fong, M. Poot, X. Han, and H. X. Tang, Phys. Rev. A **90**, 023825 (2014).
[22]C. Metzger, M. Ludwig, C. Neuenhahn, A. Ortlieb, I. Favero, K. Karrai, and F. Marquardt, Phys. Rev. Lett. **101**, 133903 (2008).
[23]W. C. Jiang and Q. Lin, Sci. Rep. **6**, 36920 (2016).
[24]W. C. Jiang, X. Lu, J. Zhang, and Q. Lin, Opt. Express **20**, 15991 (2012).
[25]X. Luan, Y. Huang, Y. Li, J. F. McMillan, J. Zheng, S.-W. Huang, P.-C. Hsieh, T. Gu, D. Wang, and A. Hati, Sci. Rep. **4**, 6842 (2014).